THE JOURNAL OF PHYSICAL CHEMISTRY A
A JOURNAL OF THE AMERICAN CHEMICAL SOCIETY

pubs.acs.org/JPCA

Article

Effects of the Intramolecular Group and Solvent on Vibrational Coupling Modes and Strengths of Fermi Resonances in Aryl Azides: A DFT Study of 4-Azidotoluene and 4-Azido-*N*-phenylmaleimide

Sathya M. Perera, Tenyu Aikawa, Sarah E. Shaner, Sean D. Moran, and Lichang Wang*

Cite This: *J. Phys. Chem. A* 2023, 127, 8911−8921

Read Online

ACCESS | Metrics & More | Article Recommendations | Supporting Information

ABSTRACT: The high transition dipole strength of the azide asymmetric stretch makes aryl azides good candidates as vibrational probes (VPs). However, aryl azides have complex absorption profiles due to Fermi resonances (FRs). Understanding the origin and the vibrational modes involved in FRs of aryl azides is critically important toward developing them as VPs for studies of protein structures and structural changes in response to their surroundings. As such, we studied vibrational couplings in 4-azidotoluene and 4-azido-*N*-phenylmaleimide in two solvents, *N*,*N*-dimethylacetamide and tetrahydrofuran, to explore the origin and the effects of intramolecular group and solvent on the FRs of aryl azides using density functional theory (DFT) calculations with the B3LYP functional and seven basis sets, 6-31G(d,p), 6-31+G(d,p), 6-31++G(d,p), 6-311G(d,p), 6-311+G(d,p), 6-311++G(d,p), and 6-311++G(df,pd). Two combination bands consisting of the azide symmetric stretch and another mode form strong FRs with the azide asymmetric stretch for both molecules. The FR profile was altered by replacing the methyl group with maleimide. Solvents change the relative peak position and intensity more significantly for 4-azido-*N*-phenylmaleimide, which makes it a more sensitive VP. Furthermore, the DFT results indicate that a comparison among the results from different basis sets can be used as a means to predict more reliable vibrational spectra.

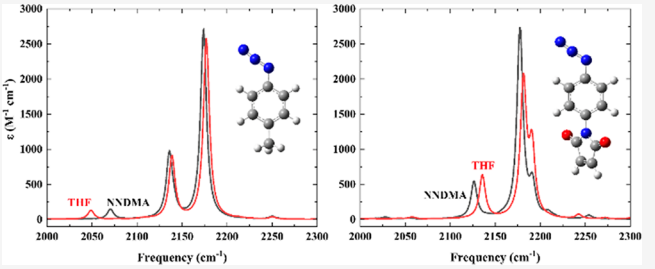

1. INTRODUCTION

Vibrational spectroscopy is a powerful tool for understanding the structures and dynamics of biological macromolecules in solution because experimentally observed frequencies and lineshapes depend on local electric field environments, solvation, and coupling between vibrational chromophores.[1,2] The intrinsic modes of proteins, peptides, and nucleic acids can be used to extract secondary structure information using linear (FTIR) and multidimensional (2D IR) methods.[3,4] It is often desirable to examine more localized phenomena, such as the polar environments of enzyme active sites or the hydration dynamics on the surfaces of proteins. Because individual native chromophores (amino acids, DNA/RNA bases) are typically not resolvable, non-natural vibrational probes (VPs) that absorb in a clear region of the mid-IR spectrum (∼1800−2300 cm^{-1}) are used.[5−8] A vast array of clear window VPs have been incorporated into proteins, including carbon−deuterium (C−D) bonds, alkynes (C≡C), nitriles (−CN), thiocyanates (−SCN), cyanamides (−NCN), azides (−N3), and various transition metal carbonyl complexes, M(CO)$_n$.[9−31] Experimental applications of these VPs face two major challenges. First, it is necessary to understand their behaviors in isolation and in simpler solvent systems to interpret the influence of the biomolecular environment on their spectra. Second, it is necessary to select a VP that reports the desired information. Theoretical and computational methods are an increasingly important complement in both regards, but any useful computational method must provide assignments and predictions that are robust to VP structures and environments.

From an experimental perspective, the characteristics of an "ideal" VP include a large transition dipole strength, sensitivity to the surrounding environment, a long vibrational lifetime, chemical stability, and a small perturbative effect on the macromolecular structure. Large transition dipole strengths facilitate the detection of VPs at working concentrations in the micromolar to low-millimolar range with high signal-to-noise ratios. For example, the major challenge of using C−D, C≡C, and −CN based VPs is their low transition dipole strength compared to those of metal−carbonyl complexes and azide-based VPs. The sensitivity to the environment arises from frequency shifts imposed by local electrostatic interactions, which are the source of solvatochromism and inhomogeneous broadening in the experimental spectra. Although the

Received: September 20, 2023
Revised: September 23, 2023
Published: October 11, 2023

https://doi.org/10.1021/acs.jpca.3c06312
J. Phys. Chem. A 2023, 127, 8911−8921

inhomogeneous contribution to a VP's total line width is convoluted with relaxation effects in linear (e.g., FTIR) spectra, 2D IR methods allow deconvolution of intrinsic and solvent-dependent effects.[1,32] Long vibrational lifetimes provide increased resolution by narrowing the homogeneous line width and simultaneously allow access to larger temporal windows in time-resolved experiments. A variety of studies have shown that the incorporation of a heavy atom (S, Si, Se, Sn) or isotope (^{15}N) into VPs can increase their lifetimes by factors ranging from ∼2 to >100.[33−36] In addition to these factors, steric perturbative effects, solvothermal stability, and the sensitivity of the VP must be considered when determining the appropriate VP for a specific application. Levin et al. have reported the relative ranking of VPs based on these parameters and found that transition metal−carbonyl compounds are least favorable in terms of their bulkiness, which can produce undesired perturbations to the protein structure, counteracting their favorability in terms of transition dipole strength and lifetime.[37] Isonitrile probes have desirable traits such as high transition dipole strength, sensitivity to the H-bonding environment, and comparatively longer vibrational lifetimes, but they are chemically unstable under acidic conditions.[38]

One additional barrier to the application of certain VPs is the separation of environmental (solvent) effects from features arising from intramolecular vibrational coupling and energy transfer. Commonly used VPs such as −CN, C≡C, and metals bearing a single carbonyl moiety have frequencies far from other modes, and their isolation minimizes coupling effects to produce single Voigt-shaped peaks in the transparent window. This is advantageous because static and time-dependent lineshapes can be readily interpreted using fluctuation−dissipation relations, typically via the application of Kubo line shape theory.[1,32,39] Other VPs such as azides and metal polycarbonyls have multiple near-lying transitions that are susceptible to coupling effects, which cause splitting in linear spectra and the appearance of cross-peaks in 2D IR spectra. In metal polycarbonyls, coupling between near-degenerate C≡O stretches dominates, and although multiple features are observed, they can still be understood from calculations using a minimal set of chromophores with a known geometry.[31,40−42] In azides (particularly aryl-azides, e.g., *p*-azidophenylalanine[21]), "accidental" Fermi resonances (FRs) between the azide antisymmetric stretch (∼2100 cm^{-1}) and lower-lying vibrations are common. FRs occur when anharmonic coupling between a bright mode (e.g., the azide fundamental) and near-degenerate, symmetry-matched overtones or combinations allow the latter to "borrow" oscillator strength, resulting in a complex absorption profile. This phenomenon makes Fermi resonant small molecules sensitive probes of the environment, in part because solvation effects (particularly H-bonding) differ between functional groups.[43] In the case of azide VPs, the involvement of low-lying modes in a denser region of state space presents a difficult analytical problem because it is not clear, a priori, which of them are coupled to the azide fundamental, and thus, how to interpret environmentally sensitive changes in the spectrum.[44−46] For this reason, aryl-azides have largely been avoided and efforts have been made to eliminate FRs to optimize them for experimental studies.[47−50]

In principle, it should be possible to leverage FRs of (aryl) azides to gain further insight into fluctuating molecular environments if their complex spectra can be assigned and predicted. To do so, it is necessary to account for the intrinsic intramolecular modes, as well as how they respond to solvation. Due to the importance of the FRs in vibrational energy transfer in proteins[51] and of understanding vibrational couplings in FRs on providing additional information on protein environment and dynamics,[43] herein, we explore the contributions of aryl ring substitution and solvation to the vibrational spectra of two aryl-azide VP analogs (Figure 1)

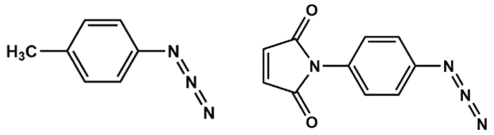

Figure 1. Chemical structures of 4-azidotoluene (left) and 4-azido-*N*-phenylmaleimide (right).

using density functional theory (DFT). The first VP analog, 4-azidotoluene, mimics *p*-azidophenylalanine, which has been studied previously and used as a VP in place of Phe and Tyr residues in proteins.[52,53] The second VP analog, 4-azido-*N*-phenylmaleimide, contains a thiol-reactive maleimide substituent that could allow post-translational attachment to cysteines in analogy to established metal−carbonyl VPs and fluorophores.[31,54] An initial version of this work was deposited in ChemRxiv on October 16, 2022.[55]

Recently, 4-azido-L-phenylalanine, the unnatural amino acid modified with an azide moiety, has been studied experimentally and theoretically[30,49,52,53,56,57] In addition, aryl azides have been explored as phosphine-activated switches for small molecule function.[58] Because of their wide application potentials, the synthesis of aryl azides is well developed.[59] Therefore, it is important to explore the vibrational modes involved in FRs and understand the effects of intramolecular groups on the FR profiles of aryl azides, as an intramolecular group replaced by or bonded with other groups can change the structure of the molecule[60,61] as well as vibrational signature.[61] In this work, we report the DFT results of the vibrational spectra of 4-azidotoluene and 4-azido-*N*-phenylmaleimide. 4-Azidotoluene is a simple analogue to 4-azido-L-phenylalanine that has been studied previously.[49,52,53,56,57] Moreover, *N*-phenyl maleimide has been studied as a substrate for Old Yellow Enzyme.[62] Since this molecule has extended conjugation and experiences greater sensitivity to energy transfer through FRs with less spectral complexity than other aryl azides, 4-azido-*N*-phenylmaleimide was also studied in this work.

Studying these two aryl azide compounds also provides an opportunity to understand the impact of intramolecular interactions on the FRs. Moreover, as VP needs to be sensitive to its environment as a probe, DFT calculations were carried out in two solvents, *N*,*N*-dimethylacetamide (NNDMA) and tetrahydrofuran (THF), to investigate the sensitivity of FRs to the solvent environment. These solvents do not generate hydrogen bonds and thus allow the use of the solvent model in DFT calculations rather than the explicit treatments of solvent molecules.[63] The B3LYP functional was used in our DFT calculations, as Barone has shown that the B3LYP exchange and correlational functional offers an excellent compromise between accuracy and computational cost and provides satisfactory results for studying the vibrational spectroscopic details of small organic molecules.[64] We note that B3LYP results may not be accurate enough to predict the resonances due to the shift of frequencies, and therefore, caution is needed

https://doi.org/10.1021/acs.jpca.3c06312
J. Phys. Chem. A 2023, 127, 8911−8921

in interpreting the calculated IR spectra. In the DFT studies of 4-azido-L-phenylalanine and its derivatives, the B3LYP functional was used in both studies that predicted different couplings using different basis sets, 6-311++G(df,pd)[49] and 6-311+G(d,p).[56] There are no systematic examinations on how the resonances in IR spectra are affected by basis sets.[65] In this work, we employed seven basis sets, namely, 6-31G(d,p), 6-31+G(d,p), 6-31++G(d,p), 6-311G(d,p), 6-311+G(d,p), 6-311++G(d,p), and 6-311++G(df,pd) in the DFT calculations to determine the basis set dependence in the absorption profile of the molecules, as shown in Figure 1. Furthermore, in addition to the cubic force constant, we also used the third-order Fermi resonance parameter (TFR)[66,67] to characterize the FRs.

2. COMPUTATIONAL DETAILS

DFT calculations were carried out on two aryl azide compounds (Figure 1) using the Gaussian 16 computational package.[68] The two molecules were built using GaussView6 that interfaces with Gaussian 16 software. While 4-azidotoluene is a rigid organic small molecule and can be built uniquely in GaussView, there are two 4-azido-*N*-phenylmaleimide rotational conformers and they have very similar IR spectra.[69] In this work, we report and discuss only one conformer shown in Figure 1. This conformer is energetically the same as the second conformer.[69] For organic small molecules of larger size, many conformers may coexist and molecular dynamics simulations may be needed to ensure proper sampling of the conformational configuration.[70]

Three types of DFT calculations were performed for each molecule in a specific solvent environment, namely, geometry optimizations, harmonic frequency calculations, and anharmonic frequency calculations. Two solvents, NNDMA (*N*,*N*-dimethylacetamide) and tetrahydrofuran (THF), were used to understand the solvent effects on FRs. The polarizable continuum model using the integral equation formalism variant (IEFPCM) was used for the solvent effect in the DFT calculations. The solvent effect has been routinely studied in DFT calculations[71,72] and utilized in tuning aggregation of organic materials[73] for better device performances.[74−76] We note that DFT calculations were performed only in the gas phase using one basis set. No extensive gas phase calculations were performed for the following two reasons. One is that future experimental studies of these molecules are expected to be performed in solvents rather than in the gas phase. The second reason is that the vibrational frequencies are the intrinsic properties of a molecule and the environment (in the gas phase or in any solvents) will only shift the absorption wavelength and intensity, as further demonstrated from the comparison with the two gas phase results.

Each DFT calculation was performed by using B3LYP. The B3LYP functional has been widely used in vibrational studies of molecules,[77−83] and it is also used in the studies of electronic transitions in molecules[84−91] or reactions of molecules[92−96] where further tests on feasible functionals are still needed.[86,88,97] In future investigations, machine learning algorithms may also be utilized in the studies.[98−100] Seven basis sets, 6-31G(d,p), 6-31+G(d,p), 6-31++G(d,p), 6-311G(d,p), 6-311+G(d,p), 6-311++G(d,p), and 6-311++G(df,pd), were employed to investigate the sensitivity of DFT results on the basis set. The basis set dependence was studied previously for UV−vis spectra of various organic small molecules.[71,101] In this work, these basis sets were chosen to understand the perturbation of electronic properties to the sensitive vibrational couplings to gain insight into the IR spectra. Standard convergence criteria were used in the DFT calculations, that is, the self-consistent field, gradient, and energy convergence of geometry optimization were set to be 10^{-8}, 10^{-4}, and 10^{-5} a.u., respectively. Ultrafine grids were used for the numerical integration of the two-electron integrals and their derivatives. These convergence criteria have been also used in our previous work on other organic small molecules.[77,78,102−104] The harmonic frequency results showed that all optimized structures were at the minimum of the potential energy surface. The generalized second-order vibrational perturbation theory[64] was used in the anharmonic frequency calculations that were performed to understand the origin of FRs and to obtain cubic force constants of overtones and combination bands. While the method allows calculations of FRs, the accuracy of using this method to account for all degeneracies is still being tested.[105] In an anharmonic frequency calculation, we provided the fundamental mode of interest, i.e., the azide asymmetric stretch, which can be identified from the harmonic frequency calculation. The calculated harmonic and anharmonic frequencies of the selected normal modes of the two molecules in NNDMA and THF are provided in Tables S1−S4. All IR spectra were obtained at room temperature (298.15K) and 1 atm, which are the default selections for obtaining IR spectra of molecules.

We used both cubic coupling constants K_{ijk} and third-order Fermi resonance parameter (TFR)[66,67] to determine the FRs. TFR for the triple of modes i, j, and k was obtained by

$$\mathrm{TFR} = \frac{|K_{ijk}|}{\Delta\omega} \tag{1}$$

$$\Delta\omega = |\omega_i + \omega_j - \omega_k| \tag{2}$$

where k is fundamental and i and j are combination band or overtone modes when $i = j$, respectively. The unit of cubic force constants is cm^{-1}, which has been widely used in the calculations[49,56] since the 1950s.[106] As such, the TFR is dimensionless. Modes are considered resonant when the TFR is of order ∼1 or larger. To make sure all the possible couplings are included, we searched all the vibrational peaks within ±130 cm^{-1} from the fundamental vibration of interest. Coupled with the cubic coupling constants, the TFR value provides insights into what possible FRs are present in the complex absorption profile of aryl azides more reliably than using cubic force constants only. Therefore, we used both the TFR and cubic force constant to measure the couplings. In this work, we investigated the influence of basis sets by comparing four parameters: peak intensity, peak position relative to the fundamental vibration, cubic force constant, and TFR value. The relative peak position ($\Delta\omega'$) is calculated as

$$\Delta\omega' = \omega_{ij} - \omega_k \tag{3}$$

where ω_{ij} and ω_k are wavenumbers of combination band or overtone and fundamental vibration, respectively.

3. RESULTS AND DISCUSSION

To understand the origin of the FRs and the impact of functional groups as well as solvent on FRs of aryl azides, we obtained DFT results on two molecules, 4-azidotoluene and 4-azido-*N*-phenylmaleimide, in two solvents, NNDMA and THF using the B3LYP functional with seven basis sets. In what

https://doi.org/10.1021/acs.jpca.3c06312
J. Phys. Chem. A 2023, 127, 8911−8921

follows, we present the results of 4-azidotoluene in NNDMA, followed by 4-azido-*N*-phenylmaleimide in NNDMA and a discussion of the effect of replacing the methyl group with maleimide. Finally, we present the results of different solvents to explore the impact of the solvent on FRs of aryl azides.

3.1. 4-Azidotoluene in NNDMA. There are 17 atoms in 4-azidotoluene. This means that there are 45 fundamental vibrational modes. We obtained the IR spectra from both harmonic and anharmonic frequency calculations of the optimized 4-azidotoluene in NNDMA using seven basis sets: 6-31G(d,p), 6-31+G(d,p), 6-31++G(d,p), 6-311G(d,p), 6-311+G(d,p), 6-311++G(d,p), and 6-311++G(df,pd). Figure S1 of the Supporting Information shows the harmonic spectrum of 4-azidotoluene using the 6-311+G(d,p) basis set. The highest intensity peak corresponds to the azide asymmetric stretching vibration, which is located at 2213.7 cm^{-1} with a molar absorptivity coefficient of ~6000 M^{-1} cm^{-1}. Indeed, this azide asymmetric stretching vibration (Mode 38) is the only visible fundamental vibration within the transparent window (~1800−2300 cm^{-1}). Mode 30 has the second highest molar absorptivity coefficient with ε over 1000 M^{-1} cm^{-1}, which indicates that transition dipole strength or population density of Modes 38 and 30 are relatively high. All other fundamentals have an intensity less than 1000 M^{-1} cm^{-1}. Table S1 shows the position and intensity of high intensity peaks for 4-azidotoluene in NNDMA obtained from the B3LYP/6-311+G(d,p) calculations. Figure S1 also presents the anharmonic vibrations, and it shows that the intensities of the anharmonic vibrations are lower than those of the harmonic vibrations. In the harmonic analysis, only a single peak within the transparent window is observed, while in the anharmonic spectrum, there are several peaks within the transparent window. However, only one fundamental, Mode 38, is present, and the other peaks are combination bands or overtones and are the result of coupling with Mode 38.

To gain deeper insights into the vibrational coupling and FRs, we plotted the vibrational spectra obtained using various basis sets in Figure 2. Furthermore, we provided the peak intensities, peak positions relative to the fundamental vibration, cubic force constants (K_{ijk}), and TFR values of combination bands or overtones that can potentially be in resonance with the azide asymmetric stretch, as shown in Figure S2. Although there are more than one hundred vibrational transitions within the transparent window, only a few modes show visible intensity or vibrational coupling strength. Unexpectedly, the combination band Comb(22,26) from the B3LYP/6-31G(d,p) calculation has the highest intensity (~1200 km mol^{-1}), and the fundamental vibration has a much lower intensity [see Figure S2d]. This result was found to be erratic and will be discussed at the end of this section. In what follows, we exclude the results from this calculation. DFT results for the remaining basis sets show azide asymmetric stretch intensities greater than 740 km mol^{-1}. Comb(18,30) and Comb(15,30) have the second and third highest intensities of ~270 and ~35 km mol^{-1}, respectively, for more diffused basis sets, i.e., 6-31+G(d,p), 6-31++G(d,p), 6-311+G(d,p), and 6-311++G-(d,p). Moreover, Comb(17,30) has a lower than 30 km mol^{-1} intensity. The overtone mode, Over(25), is very far away in frequency from Mode 38 and has an intensity of ~10 km mol^{-1}. All other vibrational modes have an intensity of less than 10 km mol^{-1}. When a combination band or overtone mode is very close to the fundamental vibration (Mode 38), and the cubic force constant is greater than 1 cm^{-1}, then there is a great chance that that combination mode is resonant with Mode 38. On the other hand, when a particular mode is very far away from Mode 38, then to generate FR, it must have a higher cubic constant.

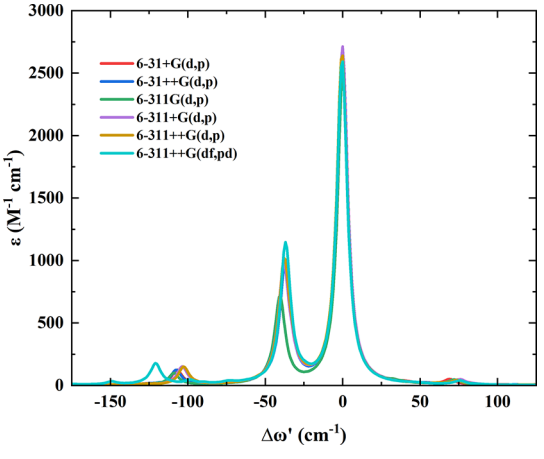

Figure 2. Vibrational spectra relative to Mode 38 of 4-azidotoluene in NNDMA from B3LYP calculations with various basis sets.

Although peak positions and intensities vary for different basis sets, the FR profiles in Figure 2 look similar. The left peak around −100 cm^{-1} is Comb(15, 30), which has the highest cubic force constant of ~55 cm^{-1}. As it is far away from Mode 38, it does not form FR with Mode 38 but coupling is visible. The same is true for Over(25), which is more than 50 cm^{-1} to the right of Mode 38. The band to the left of Mode 38 includes two combination bands, Comb(18,30) and Comb(17,30). Comb(18,30) has the second highest coupling constant, ~ 48 cm^{-1}, while Comb(17,30) has a cubic force constant of less than 10 cm^{-1}. We mention that the cubic force constants for Comb(18,30) and Comb(17,30) from B3LYP/6-311++(df,pd) are quite different from those obtained with the other basis sets. This more polarized basis set shows an increased cubic force constant of ~31 cm^{-1} for Comb(17,30) and a decreased cubic force constant of ~32 cm^{-1} for Comb(18,30). This erratic data will also be discussed at the end of this section.

To further confirm FRs with Mode 38, we calculated TFR values of various combination or overtone bands, and the results are summarized in Table S5. If the TFR value is higher than 1, then the particular combination band or overtone is said to be strongly coupled with the fundamental vibration. A TFR between 1 and 0.3 cm^{-1} indicates that the overtone or combination band is weakly coupled to the fundamental vibration. Data in Table S5 show that Comb(18,30) has a TFR value greater than 1 cm^{-1}, which further confirms that Comb(18,30) is strongly coupled to the azide asymmetric stretch, Mode 38, and thus forms a strong FR. Comb(17,30) has a TFR value of ~0.5 cm^{-1} which is weakly coupled to Mode 38 and forms a weak FR with Mode 38. Both Comb(15,30) and Over(25) also have TFR values of ~0.6 and ~0.4 cm^{-1}, respectively, but these bands are very far away in frequency from Mode 38; therefore, they do not form FRs but still weakly couple to the azide asymmetric stretch. The vibrational modes that form the FRs or are coupled with Mode 38, as discussed above, are shown in Figure 3.

Compared with the DFT studies for 4-azido-L-phenylalanine derivative, Ac-p-N_3−Phe-OMe,[56] the current DFT results

https://doi.org/10.1021/acs.jpca.3c06312
J. Phys. Chem. A 2023, 127, 8911−8921

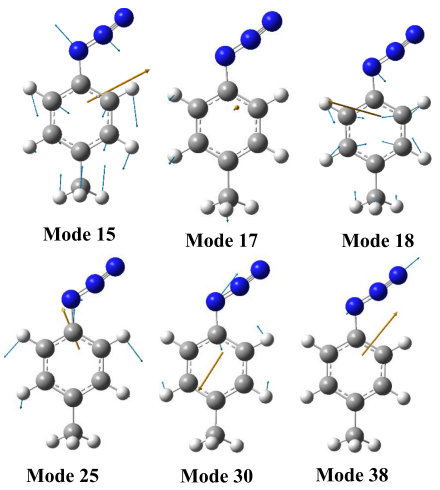

Figure 3. Vibrational modes of combination or overtone bands that couple with the azide asymmetric stretch (Mode 38) in 4-azidotoluene in NNDMA. Modes 15, 17, 18, 25, and 30 correspond to N_3 bend, sp^2 CH in-plane, sp^3 CH out-of-plane, benzene ring vibrations; CH out-of-plane vibrations; N_3 bend, sp^2 CH in-plane, sp^3 CH out-of-plane, benzene ring vibrations; N_3 Sym stretch, sp^2 in-plane, benzene ring vibrations, CN stretch; N_3 Sym stretch, sp^2 CH in-plane, benzene ring vibrations, CN stretch, respectively. Blue arrows indicate the motions of atoms and brown arrows are the direction of dipole.

show that the modes involved in FRs are unchanged upon replacing the alanine moiety with a methyl group. Both combination bands contain the same mode, Mode 30 here and denoted as Mode 63 in Ac-p-N_3-Phe-OMe.[56] However, DFT results for FRs in 4-azido-L-phenylalanine involve 4 different modes, Comb(42,20) and Comb(41,21).[49] While both molecules, 4-azido-L-phenylalanine and 4-azidotoluene, have two combination bands that form FRs with the fundamental mode, the difference in mode involvements from 4-azido-L-phenylalanine may be partially due to the basis set being used, which will be explained below. The results are encouraging as they illustrated the robustness of FRs in both molecules, i.e., two combination bands involved in FRs despite different intramolecular groups, which offers foundation for systematic tuning of VPs.

Finally, we mention the dependence of DFT results on the basis set. Most of the DFT results using the 7 basis sets predicted similar trends and modes involved. Two basis sets, 6-31G(d,p) and 6-311++(df,pd), generate erratic results. This is clearly demonstrated when we compare the results of intensity and cubic force constant. In the case of 6-31G(d,p), it seems the intensity for Comb(22,26) and that of Mode 38 are switched [see Figure S2a]. To verify this, we performed B3LYP/6-31G(d,p) anharmonic frequency calculation using a B3LYP/6-31+G(d,p) optimized structure, and the data seem to be fine. Likewise, B3LYP/6-31+G(d,p) anharmonic frequency calculation using a B3LYP/6-31+G(d,p) optimized structure also provided reasonable results. For 6-311++(df,pd), cubic force constants for Comb(18,30) and Comb(17,30) are mixed in comparison with the results from the other basis sets [see Figure S2b]. Similar basis set swap calculations confirmed that numerical errors led to erroneous results. This suggests that it is useful to perform calculations using a few basis sets for reliable predictions. This conclusion is further supported by the other calculations to be discussed below.

3.2. 4-Azido-*N*-phenylmaleimide in NNDMA.

To understand how different functional groups interact with the azide asymmetric stretch and contribute to the FRs in the absorption profile of azide VPs, we replaced the simple methyl group in 4-azidotoluene with a maleimide moiety to form 4-azido-*N*-phenylmaleimide. 4-Azido-*N*-phenylmaleimide has 22 atoms. Hence, there are 60 fundamental vibrational modes present. Table S3 presents the DFT results for high intensity modes with molar absorptivity coefficients over 1000 M^{-1} cm^{-1}. It shows that the carbonyl stretch (Mode 52) and azide asymmetric stretch (Mode 54) have the highest intensities followed by Modes 48, 45, and 46. Figure S3 shows the harmonic and anharmonic spectra with a 6-311+G(d,p) basis set. DFT results are displayed in Figure S4a for the high-intensity vibrational transitions within the transparent window as well as some lower-intensity peaks included due to their high cubic force constant (>1 cm^{-1}) for all basis set calculations. Detailed comparisons among the results from different basis sets can be found in the discussion following Figure S4.

The spectra of 4-azido-*N*-phenylmaleimide within the transparent window from DFT calculations are depicted in Figure 4. The highest intensity peak (~800 km mol^{-1})

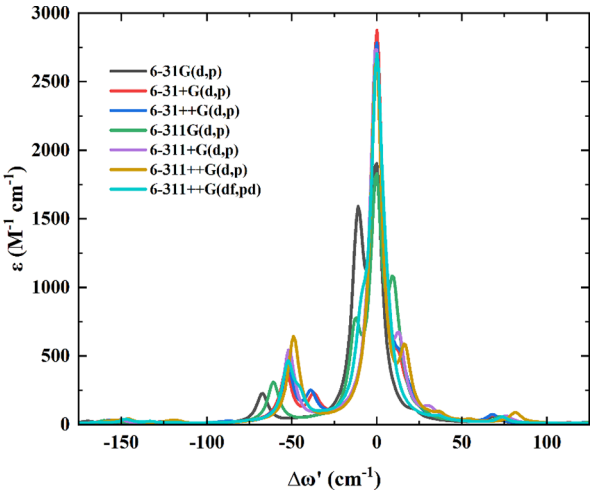

Figure 4. Vibrational spectra relative to mode 54 of 4-azido-*N*-phenylmaleimide in NNDMA from B3LYP calculations with various basis sets.

corresponds to the azide asymmetric stretch, Mode 54, and other combination bands are the result of multiple vibrational transitions that are coupled to Mode 54. In comparison to Figure 2, the spectra seem to be more basis-set-dependent, although detailed analysis shows that a rather consistent conclusion can be reached. The peaks to the right of Mode 54 by more than 50 cm^{-1} are overtone Over(39), which has an intensity of ~14 km mol^{-1} and a high cubic force constant (~37 cm^{-1}). However, it will not form FR with Mode 54 due to a small TFR value.

The absorption band to the left of mode 54 is Comb(27,45). It has a cubic force constant over 50 cm^{-1}. Third-order Fermi resonance values of each mode were calculated and shown in Table S6 to figure out whether these combinations bands or overtone can resonantly couple with the azide asymmetric stretch. TFR values increase when the magnitude of the cubic force constant increases and/or when resonance shift $\Delta\omega$ decreases. Generally, if TFR $\geq$ 1, k > 10 cm^{-1}, and $\Delta\omega'$ < 10

https://doi.org/10.1021/acs.jpca.3c06312
J. Phys. Chem. A 2023, 127, 8911−8921

cm^{-1}, then the overall coupling strength will be significant enough to result in FR between the fundamental band and the combinations bands/overtone. For instance, both Comb(27,45) and Comb(27,46) are rather far away in frequency from the fundamental vibration, but cubic force constants are so high that they can still result in FRs. Comb(27,45) and Comb(27,46) have TFR values greater than 1, indicating that they form strong FRs with the azide asymmetric stretch.

From the analysis based on cubic force constants and TFR values, all basis sets have questionable vibrational modes for identifying combination bands or overtones that can couple with azide asymmetric stretch when the TFR is <0.3. Therefore, it is less reliable in DFT predictions of weak FRs. The vibrational modes that form the FRs or coupled with Mode 54 as discussed above are shown in Figure 5.

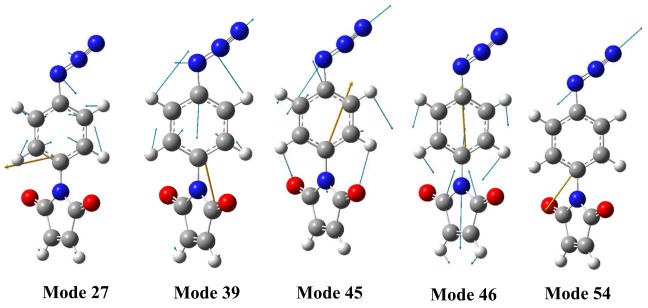

Figure 5. Vibrational modes of combination or overtone bands that couple with the azide asymmetric stretch (Mode 54) in 4-azido-*N*-phenylmaleimide in NNDMA. Modes 27, 39, 45, and 46 correspond to N_3 bend, sp^2 CH in-plane, benzene ring vibrations; N_3 Sym stretch, sp^2 in-plane, benzene ring vibrations; N_3 Sym stretch, sp^2 CH in-plane, benzene ring vibrations, CN stretch; N_3 Sym stretch, sp^2 CH in-plane, benzene ring vibrations, CN stretch, respectively. Blue arrows indicate the motions of atoms, and brown arrows are the direction of dipole.

To investigate the effect of an intramolecular group on the FR profile, we depicted the spectra of 4-azidotoluene and 4-azido-*N*-phenylmaleimide in NNDMA in Figure 6. While the two combination bands that are involved in FRs, Comb(18,30), and Comb(17,30) are located at the left of the fundamental, mode 38, in 4-azidotoluene, the two combination bands that are involved in FRs, Comb(27,45), and Comb(27,46) are located at the left and right of the fundamental, Mode 54, in 4-azido-*N*-phenylmaleimide, respectively, illustrating the effect of replacing the methyl group with maleimide.

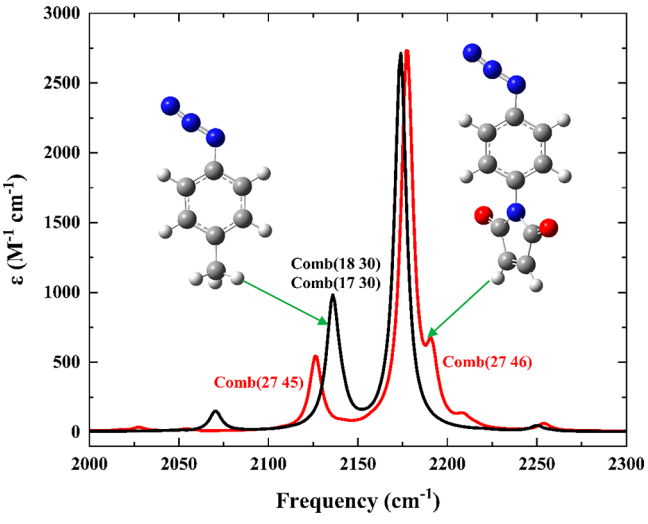

Figure 6. Vibrational spectra of 4-azidotoluene (black) and 4-azido-*N*-phenylmaleimide (red) in NNDMA from B3LYP/6-311+G(d,p) calculations.

3.3. Solvent Effects on FRs in 4-Azidotoluene and 4-Azido-*N*-phenylmaleimide. The vibrational spectra of 4-azidotoluene and 4-azido-*N*-phenylmaleimide in THF were obtained using B3LYP calculations with seven basis sets. The dielectric constants for NNDMA and THF are 37.8 and 7.6, respectively. Therefore, a comparison of the results in two solvents will provide information about the sensitivity of the IR spectra in the transparent window of these molecules to their environments. We discuss first the results of 4-azidotoluene in THF. Figure S5 and Table S2 show that Mode 38 and Mode 30 have the highest intensities in THF as in the NNDMA solvent. Figure S6 shows various properties for the vibrational modes occurring within ±130 cm^{-1} of the fundamental vibration. Figure S6a presents high-intensity vibrational modes within the transparent region. The highest intensity corresponds to the azide asymmetric stretch, mode 38. The intensity of mode 38 in THF is around 740 km mol^{-1}, which is lower than that in NNDMA. As in NNDMA, the second and third highest intensity peaks correspond to Comb(18,30) and Comb(15,30).

The intensity of Comb(17,30) in THF varies for different basis sets as it did in NNDMA. Over(25) has an intensity of ~10 km mol^{-1}, and all other vibrational modes within the transparent window have lower intensity than 10 km mol^{-1}. These observations verify that changing the solvents does not influence the identity of FRs, but the intensity of each vibrational transition in all calculations is lower with THF. According to Figure S6b, not only intensity values but also cubic force constants have similar trends in both solvents. The highest cubic force constant of ~55 cm^{-1} is observed for Comb(15,30) in all basis sets, and the second highest cubic force constant ~48 cm^{-1} is for Comb(18,30). Like in NNDMA, the cubic force constant of Comb(18,30) drops to ~36 cm^{-1}. Over(25) has ~32 cm^{-1} cubic force constant and Comb(17,30) has force constant less than 10 cm^{-1}.

The peak positions of vibrational modes are also solvent-dependent. The azide asymmetric stretch blue shifts in THF calculations. Like in NNDMA, Comb(15,30) and Over(25) are very far ($\Delta\omega'$ > 100 and >65 cm^{-1}, respectively) away energetically from mode 38, and Comb(18,30) and Comb(17,30) are positioned close. Table S7 shows TFR values for possible modes that can resonantly couple with the azide asymmetric stretch for 4-azidotoluene in a THF solvent. Here, again, Comb(18,30) has a TFR value >1 because Comb(18,30) is strongly coupled to the azide asymmetric stretch. Although both Comb(15,30) and Over(25) are far away in frequency from the fundamental vibration mode 38, they show TFR values ~0.55 and ~0.45, respectively. Therefore, both Comb(15,30) and Over(25) are weakly coupled to the azide asymmetric stretch. Also, Comb(17,30) is very weakly coupled to the azide asymmetric stretch due to its moderate cubic force constant and relative peak position. The vibrational modes that contribute to the FRs in THF are the same as those shown in Figure 3. The vibrational spectrum of 4-azido-*N*-phenylmaleimide (Figure S7) in THF shows five peaks with high intensities over 1000 M^{-1} cm^{-1}, just as in NNDMA. The properties of the combination and overtone bands that occur

https://doi.org/10.1021/acs.jpca.3c06312
J. Phys. Chem. A 2023, 127, 8911−8921

within ±135 cm^{-1} from the azide asymmetric stretch using seven basis sets are listed in Figure S8.

The intensity of the combination bands is solvent-dependent. To get deep insights into the solvent effect on the FRs, we first consider the cubic force constants, see Figure S8b. In THF, Comb(27,45) has a cubic force constant of over 50 cm^{-1}. Therefore, from the cubic force constants, we can directly see strong coupling between Comb(27,45) and the azide asymmetric stretch. The second highest cubic force constant of ∼35 cm^{-1} is Over(39). The intensities of both Comb(27,45) and Over(39) are not that high because they are very far away in frequency from the fundamental vibration.

The solvent effects on absorption profiles of 4-azidotoluene and 4-azido-*N*-phenylmaleimide can be observed in Figure 7.

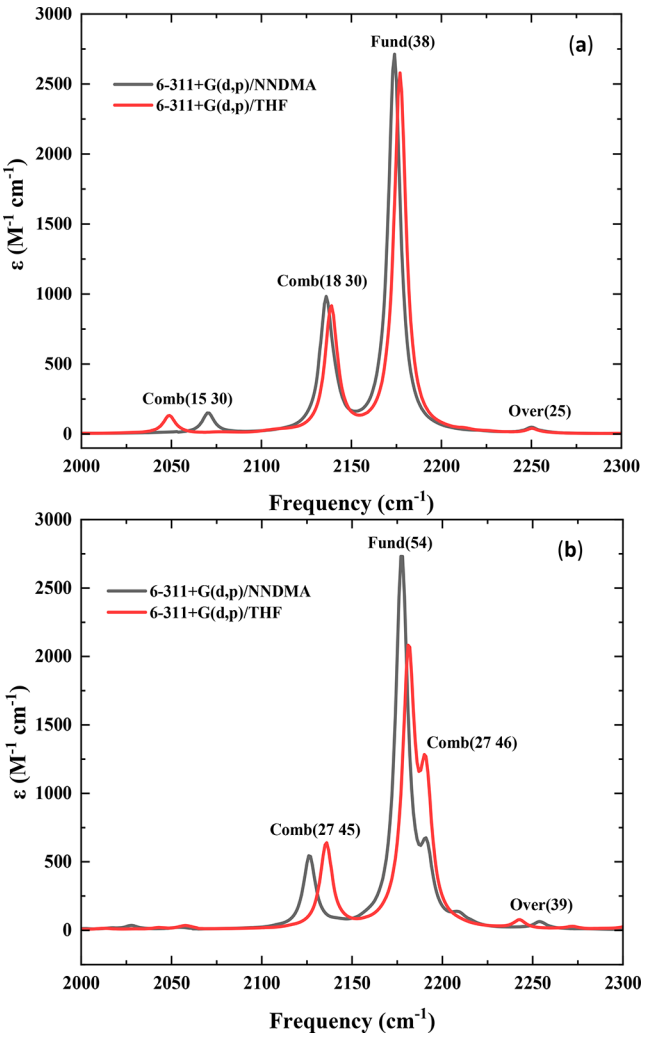

Figure 7. Vibrational spectra of 4-azidotoluene (a) and 4-azido-*N*-phenylmaleimide (b) in NNDMA and THF obtained from B3LYP/6-311+G(d,p) calculations.

THF solvent blue shifts both azide asymmetric stretch and Comb(18,30) bands in 4-azidotoluene. The intensity of these modes is lower in THF compared to NNDMA, but they have similar trends in both solvents. Figure 6 shows that when the methyl group is replaced with a maleimide group, the azide asymmetric stretch blue shifts and the azide adsorption profile is completely different from one another. Moreover, when comparing vibrational transitions that contribute to FRs, both molecules show the same vibrational modes. For example, Mode 30, 18, 25, and 17 in 4-azidotoluene are similar to modes Comb(45,46), 27, 39, and 26 in 4-azido-*N*-phenylmaleimide, respectively. Comparing the absorption profiles of 4-azidotoluene and 4-azido-*N*-phenylmaleimide in Figure 7, it seems that 4-azido-*N*-phenylmaleimide is more sensitive and thus a better VP candidate. We mention that a lot of efforts have been made to remove FRs of VP probes. The robust FR features and the sensitivity to solvents shown in this work suggest that it is a good strategy to design VPs to utilize the FRs.

It is also interesting to note that in both molecules at different solvent environments, the same combination bands and overtones are involved in FRs, as shown in Figure 7. The azide asymmetric stretch, denoted as Mode 30 in 4-azidotoluene and Mode 54 in 4-azido-*N*-phenylmaleimide, is strongly coupled with Comb(18,30), Comb(15,30), and Comb(17,30) in 4-azidotoluene and with Comb(27,45) and Comb(27,46) in 4-azido-*N*-phenylmaleimide. These combinational modes are strongly coupled with the fundamental azide asymmetric stretch through the significant azido asymmetric component in Mode 30 in Figure 3 and Mode 45 in Figure 5 or through the strong dipole coupling as in Mode 15 with Mode 38 in Figure 3 and as in Mode 27 with that in Mode 54 in Figure 5. The resonance features shown in these solvents can be observed in the gas phase as depicted in Figure S9 of the Supporting Information. We also note that the current DFT results did not include the contribution from the involvements of solvent modes, in which explicit solvent molecules are needed in the study.

Moreover, we point out that DFT results with more basis sets can be used as useful tools for reliable predictions. We provided in Tables S9−S16 the structural and electronic properties obtained with the 7 basis sets. The results do not seem to be abnormal, as shown by the predicted spectroscopic properties, such as intensity and cubic constants. These lead us to believe that the drastically different spectroscopic results are due to numerical errors introduced during calculations in obtaining the spectral properties.

Previously, comparisons between the DFT results using B3LYP functional and experimental data were made for 4-azido-L-phenylanine[49] and for paro-azidobenzonitrile.[107] The DFT results were found to be very useful in understanding the vibrations of these molecules. We performed the FTIR measurements of the potentially better VP candidate, i.e., 4-azido-*N*-phenylmaleimide, and the results are provided in Figure S10 and Table S17 of the Supporting Information. As shown in Figure S10, the computationally predicted resonance at the lower frequency with respect to the fundamental (Mode 54) was observed experimentally; however, the predicted resonances at the frequencies higher than the fundamental cannot be visible from the current experiment. We suspect that this may be due to the resolution of the IR measurements. 2D IR will be a better and interesting tool to identify these resonances as illustrated in the previous studies.[49,56] The resonance shifts were better predicted from the DFT than from the intensity, as one may expect. Finally, we point out that scaling techniques[77] may be useful to better reproduce experimental spectra and are interesting for future investigations.

https://doi.org/10.1021/acs.jpca.3c06312
J. Phys. Chem. A 2023, 127, 8911−8921

4. CONCLUSIONS

B3LYP calculations were performed on 4-azidotoluene and 4-azido-*N*-phenylmaleimide in NNDMA and THF to understand the FRs of these molecules and the solvent effect on the FRs. In both solvents, the same combination of bands and overtones is involved in FRs. In addition, those modes always include a high intensity vibrational mode. For example, in 4-azidotoluene, Mode 30 was involved in Comb(18,30), Comb(15,30), and Comb(17,30). In 4-azido-*N*-phenylmaleimide, Mode 45 and Mode 46 were involved in Comb(27,45) and Comb(27,46). Notably, Modes 30, 15, and 17 in 4-azidotoluene are similar to Modes Comb(45,46), 27, and 26 in 4-azido-*N*-phenylmaleimide, respectively. This illustrated that FRs are rather robust features and can be taken advantage of as VPs.

The azide asymmetric stretch blue shifts upon substitution of methyl with the maleimide group and solvent change from NNDMA to THF. 4-azido-*N*-phenylmaleimide shows a greater sensitivity to solvent and therefore is a better candidate as a VP than 4-azidotoluene. These results are critical for understanding the modes involved in the ongoing 2D IR measurements of these molecules. Finally, we note that 6-31+G(d,p) and 6-311+G(d,p) basis sets seem to be good choices for DFT calculations, and it is important to use multiple basis sets for reliable predictions by comparing the cubic constants and frequencies.

ASSOCIATED CONTENT

Supporting Information

The Supporting Information is available free of charge at https://pubs.acs.org/doi/10.1021/acs.jpca.3c06312.

IR spectra, cubic force constants, bond angles of molecules, and detailed discussion of basis set effects on IR spectra (PDF)

AUTHOR INFORMATION

Corresponding Author

Lichang Wang − *School of Chemical and Biomolecular Sciences, Southern Illinois University, Carbondale, Illinois 62901, United States;* orcid.org/0000-0002-6131-3532; Phone: +1 618-453-6476; Email: lwang@chem.siu.edu; Fax: +1 618-453-6408

Authors

Sathya M. Perera − *School of Chemical and Biomolecular Sciences, Southern Illinois University, Carbondale, Illinois 62901, United States;* orcid.org/0000-0003-4202-8688

Tenyu Aikawa − *School of Chemical and Biomolecular Sciences, Southern Illinois University, Carbondale, Illinois 62901, United States*

Sarah E. Shaner − *Department of Chemistry and Physics, Southeast Missouri State University, Cape Girardeau, Missouri 63701, United States;* orcid.org/0000-0002-4724-6628

Sean D. Moran − *School of Chemical and Biomolecular Sciences, Southern Illinois University, Carbondale, Illinois 62901, United States;* orcid.org/0000-0002-3762-6520

Complete contact information is available at: https://pubs.acs.org/10.1021/acs.jpca.3c06312

Notes

The authors declare no competing financial interest.

ACKNOWLEDGMENTS

This work was partially supported by the National Science Foundation (REU-DMR-1757954). We thank Dr. Tayler Hill for providing the experimental data shown in the Supporting Information. SDM acknowledges the financial support from the National Institute of General Medical Sciences of the National Institute of Health under award number R35GM119818.

REFERENCES

(1) Hamm, P.; Zanni, M. *Concepts and Methods of 2D Infrared Spectroscopy*; Cambridge University Press: Cambridge, 2011.

(2) Ghosh, A.; Ostrander, J. S.; Zanni, M. T. Watching Proteins Wiggle: Mapping Structures with Two-Dimensional Infrared Spectroscopy. *Chem. Rev.* **2017**, *117*, 10726−10759.

(3) Ganim, Z.; Chung, H. S.; Smith, A. W.; DeFlores, L. P.; Jones, K. C.; Tokmakoff, A. Amide I Two-Dimensional Infrared Spectroscopy of Proteins. *Acc. Chem. Res.* **2008**, *41*, 432−441.

(4) Le Sueur, A. L.; Horness, R. E.; Thielges, M. C. Applications of Two-Dimensional Infrared Spectroscopy. *Analyst* **2015**, *140*, 4336−4349.

(5) Thielges, M. C. Transparent Window 2D IR Spectroscopy of Proteins. *J. Chem. Phys.* **2021**, *155*, No. 040903.

(6) Ma, J.; Pazos, I. M.; Zhang, W.; Culik, R. M.; Gai, F. Site-Specific Infrared Probes of Proteins. *Annu. Rev. Phys. Chem.* **2015**, *66*, 357−77.

(7) Kim, H.; Cho, M. Infrared Probes for Studying the Structure and Dynamics of Biomolecules. *Chem. Rev.* **2013**, *113*, 5817−5847.

(8) Adhikary, R.; Zimmermann, J.; Romesberg, F. E. Transparent Window Vibrational Probes for the Characterization of Proteins with High Structural and Temporal Resolution. *Chem. Rev.* **2017**, *117*, 1927−1969.

(9) Choi, J.-H.; Oh, K.-I.; Lee, H.; Lee, C.; Cho, M. Nitrile and Thiocyanate Ir Probes: Quantum Chemistry Calculation Studies and Multivariate Least-Square Fitting Analysis. *J. Chem. Phys.* **2008**, *128*, 134506.

(10) Oh, K.-I.; Choi, J.-H.; Lee, J.-H.; Han, J.-B.; Lee, H.; Cho, M. Nitrile and Thiocyanate IR Probes: Molecular Dynamics Simulation Studies. *J. Chem. Phys.* **2008**, *128*, 154504.

(11) Choi, J.-H.; Cho, M. Vibrational Solvatochromism and Electrochromism of Infrared Probe Molecules Containing C≡O, C≡N, C = O, or C−F Vibrational Chromophore. *J. Chem. Phys.* **2011**, *134*, 154513.

(12) Chin, J. K.; Jimenez, R.; Romesberg, F. E. Direct Observation of Protein Vibrations by Selective Incorporation of Spectroscopically Observable Carbon−Deuterium Bonds in Cytochrome C. *J. Am. Chem. Soc.* **2001**, *123*, 2426−2427.

(13) Zimmermann, J.; Gundogdu, K.; Cremeens, M. E.; Bandaria, J. N.; Hwang, G. T.; Thielges, M. C.; Cheatum, C. M.; Romesberg, F. E. Efforts toward Developing Probes of Protein Dynamics: Vibrational Dephasing and Relaxation of Carbon−Deuterium Stretching Modes in Deuterated Leucine. *J. Phys. Chem. B* **2009**, *113*, 7991−7994.

(14) Lam, Z.; Kong, K. V.; Olivo, M.; Leong, W. K. Vibrational Spectroscopy of Metal Carbonyls for Bio-Imaging and -Sensing. *Analyst* **2016**, *141*, 1569−1586.

(15) Deiters, A.; Schultz, P. G. In Vivo Incorporation of an Alkyne into Proteins in Escherichia Coli. *Bioorg. Med. Chem. Lett.* **2005**, *15*, 1521−1524.

(16) Zheng, M. L.; Zheng, D. C.; Wang, J. Non-Native Side Chain Ir Probe in Peptides: Ab Initio Computation and 1D and 2D IR Spectral Simulation. *J. Phys. Chem. B* **2010**, *114*, 2327−2336.

(17) Lee, G.; Kossowska, D.; Lim, J.; Kim, S.; Han, H.; Kwak, K.; Cho, M. Cyanamide as an Infrared Reporter: Comparison of Vibrational Properties between Nitriles Bonded to N and C Atoms. *J. Phys. Chem. B* **2018**, *122*, 4035−4044.

(18) Fafarman, A. T.; Webb, L. J.; Chuang, J. I.; Boxer, S. G. Site-Specific Conversion of Cysteine Thiols into Thiocyanate Creates an IR Probe for Electric Fields in Proteins. *J. Am. Chem. Soc.* **2006**, *128*, 13356−13357.

(19) Getahun, Z.; Huang, C. Y.; Wang, T.; De León, B.; DeGrado, W. F.; Gai, F. Using Nitrile-Derivatized Amino Acids as Infrared Probes of Local Environment. *J. Am. Chem. Soc.* **2003**, *125*, 405−411.
(20) Waegele, M. M.; Tucker, M. J.; Gai, F. 5-Cyanotryptophan as an Infrared Probe of Local Hydration Status of Proteins. *Chem. Phys. Lett.* **2009**, *478*, 249−253.
(21) Fafarman, A. T.; Boxer, S. G. Nitrile Bonds as Infrared Probes of Electrostatics in Ribonuclease S. *J. Phys. Chem. B* **2010**, *114*, 13536−13544.
(22) Thielges, M. C.; Axup, J. Y.; Wong, D.; Lee, H. S.; Chung, J. K.; Schultz, P. G.; Fayer, M. D. Two-Dimensional IR Spectroscopy of Protein Dynamics Using Two Vibrational Labels: A Site-Specific Genetically Encoded Unnatural Amino Acid and an Active Site Ligand. *J. Phys. Chem. B* **2011**, *115*, 11294−11304.
(23) Bazewicz, C. G.; Lipkin, J. S.; Smith, E. E.; Liskov, M. T.; Brewer, S. H. Expanding the Utility of 4-Cyano-L-Phenylalanine as a Vibrational Reporter of Protein Environments. *J. Phys. Chem. B* **2012**, *116*, 10824−10831.
(24) Shi, L.; Liu, X.; Shi, L.; Stinson, H. T.; Rowlette, J.; Kahl, L. J.; Evans, C. R.; Zheng, C.; Dietrich, L. E. P.; Min, W. Mid-Infrared Metabolic Imaging with Vibrational Probes. *Nat. Methods* **2020**, *17*, 844−851.
(25) Cai, K.; Liu, J.; Liu, Y.; Chen, F.; Yan, G.; Lin, H. Application of a Transparent Window Vibrational Probe (Azido Probe) to the Structural Dynamics of Model Dipeptides and Amyloid B-Peptide. *Spectrochim Acta, Part A* **2020**, *227*, No. 117681.
(26) Chalyavi, F.; Adeyiga, O.; Weiner, J. M.; Monzy, J. N.; Schmitz, A. J.; Nguyen, J. K.; Fenlon, E. E.; Brewer, S. H.; Odoh, S. O.; Tucker, M. J. 2d-Ir Studies of Cyanamides (NCN) as Spectroscopic Reporters of Dynamics in Biomolecules: Uncovering the Origin of Mysterious Peaks. *J. Chem. Phys.* **2020**, *152*, No. 074201.
(27) Gai, X. S.; Coutifaris, B. A.; Brewer, S. H.; Fenlon, E. E. A Direct Comparison of Azide and Nitrile Vibrational Probes. *Phys. Chem. Chem. Phys.* **2011**, *13*, 5926−5930.
(28) Lee, H.; Choi, J.-H.; Cho, M. Vibrational Solvatochromism and Electrochromism of Cyanide, Thiocyanate, and Azide Anions in Water. *Phys. Chem. Chem. Phys.* **2010**, *12*, 12658.
(29) Wolfshorndl, M. P.; Baskin, R.; Dhawan, I.; Londergan, C. H. Covalently Bound Azido Groups Are Very Specific Water Sensors, Even in Hydrogen-Bonding Environments. *J. Phys. Chem. B* **2012**, *116*, 1172−1179.
(30) Bazewicz, C. G.; Liskov, M. T.; Hines, K. J.; Brewer, S. H. Sensitive, Site-Specific, and Stable Vibrational Probe of Local Protein Environments: 4-Azidomethyl-L-Phenylalanine. *J. Phys. Chem. B* **2013**, *117*, 8987−8993.
(31) Woys, A. M.; Mukherjee, S. S.; Skoff, D. R.; Moran, S. D.; Zanni, M. T. A Strongly Absorbing Class of Non-Natural Labels for Probing Protein Electrostatics and Solvation with FTIR and 2D IR Spectroscopies. *J. Phys. Chem. B* **2013**, *117*, 5009−5018.
(32) Kwak, K.; Park, S.; Finkelstein, I. J.; Fayer, M. D. Frequency-Frequency Correlation Functions and Apodization in Two-Dimensional Infrared Vibrational Echo Spectroscopy: A New Approach. *J. Chem. Phys.* **2007**, *127*, 124503.
(33) Kossowska, D.; Lee, G.; Han, H.; Kwak, K.; Cho, M. Simultaneous Enhancement of Transition Dipole Strength and Vibrational Lifetime of an Alkyne Ir Probe Via Π-D Backbonding and Vibrational Decoupling. *Phys. Chem. Chem. Phys.* **2019**, *21*, 24919−24925.
(34) Kossowska, D.; Park, K.; Park, J. Y.; Lim, C.; Kwak, K.; Cho, M. Rational Design of an Acetylenic Infrared Probe with Enhanced Dipole Strength and Increased Vibrational Lifetime. *J. Phys. Chem. B* **2019**, *123*, 6274−6281.
(35) Park, K.-H.; Jeon, J.; Park, Y.; Lee, S.; Kwon, H.-J.; Joo, C.; Park, S.; Han, H.; Cho, M. Infrared Probes Based on Nitrile-Derivatized Prolines: Thermal Insulation Effect and Enhanced Dynamic Range. *J. Phys. Chem. Lett.* **2013**, *4*, 2105−2110.
(36) Chalyavi, F.; Schmitz, A. J.; Fetto, N. R.; Tucker, M. J.; Brewer, S. H.; Fenlon, E. E. Extending the Vibrational Lifetime of Azides with Heavy Atoms. *Phys. Chem. Chem. Phys.* **2020**, *22*, 18007−18013.
(37) Levin, D. E.; Schmitz, A. J.; Hines, S. M.; Hines, K. J.; Tucker, M. J.; Brewer, S. H.; Fenlon, E. E. Synthesis and Evaluation of the Sensitivity and Vibrational Lifetimes of Thiocyanate and Selenocyanate Infrared Reporters. *RSC Adv.* **2016**, *6*, 36231−36237.
(38) Maj, M.; Ahn, C.; Błasiak, B.; Kwak, K.; Han, H.; Cho, M. Isonitrile as an Ultrasensitive Infrared Reporter of Hydrogen-Bonding Structure and Dynamics. *J. Phys. Chem. B* **2016**, *120*, 10167−10180.
(39) Kubo, R. A Stochastic Theory of Line Shape. *Adv. Chem. Phys.* **1969**, *16*, 101−127.
(40) Khalil, M.; Demirdöven, N.; Tokmakoff, A. Vibrational Coherence Transfer Characterized with Fourier-Transform 2d Ir Spectroscopy. *J. Chem. Phys.* **2004**, *121*, 362−373.
(41) Baiz, C. R.; Kubarych, K. J.; Geva, E. Molecular Theory and Simulation of Coherence Transfer in Metal Carbonyls and Its Signature on Multidimensional Infrared Spectra. *J. Phys. Chem. B* **2011**, *115*, 5322−5339.
(42) King, J. T.; Kubarych, K. J. Site-Specific Coupling of Hydration Water and Protein Flexibility Studied in Solution with Ultrafast 2D-IR Spectroscopy. *J. Am. Chem. Soc.* **2012**, *134*, 18705−18712.
(43) Rodgers, J. M.; Abaskharon, R. M.; Ding, B.; Chen, J.; Zhang, W.; Gai, F. Fermi Resonance as a Means to Determine the Hydrogen-Bonding Status of Two Infrared Probes. *Phys. Chem. Chem. Phys.* **2017**, *19*, 16144−16150.
(44) Dutta, S.; Cook, R. J.; Houtman, J. C. D.; Kohen, A.; Cheatum, C. M. Characterization of Azido-Nad$^+$ to Assess Its Potential as a Two-Dimensional Infrared Probe of Enzyme Dynamics. *Anal. Biochem.* **2010**, *407*, 241−246.
(45) Nydegger, M. W.; Dutta, S.; Cheatum, C. M. Two-Dimensional Infrared Study of 3-Azidopyridine as a Potential Spectroscopic Reporter of Protonation State. *J. Chem. Phys.* **2010**, *133*, 134506.
(46) Lieber, E.; Rao, C. N. R.; Thomas, A. E.; Oftedahl, E.; Minnis, R.; Nambury, C. V. N. Infrared Spectra of Acid Azides, Carbamyl Azides and Other Azido Derivatives: Anomalous Splittings of the N3 Stretching Bands. *Spectrochim. Acta* **1963**, *19*, 1135−1144.
(47) Nydegger, M. W.; Dutta, S.; Cheatum, C. M. Two-Dimensional Infrared Study of 3-Azidopyridine as a Potential Spectroscopic Reporter of Protonation State. *J. Chem. Phys.* **2010**, *133*, 134506.
(48) Lipkin, J. S.; Song, R.; Fenlon, E. E.; Brewer, S. H. Modulating Accidental Fermi Resonance: What a Difference a Neutron Makes. *J. Phys. Chem. Lett.* **2011**, *2*, 1672−1676.
(49) Zhang, J.; Wang, L.; Zhang, J.; Zhu, J.; Pan, X.; Cui, Z.; Wang, J.; Fang, W.; Li, Y. Identifying and Modulating Accidental Fermi Resonance: 2D IR and DFT Study of 4-Azido-L-Phenylalanine. *J. Phys. Chem. B* **2018**, *122*, 8122−8133.
(50) Lipkin, J. S.; Song, R.; Fenlon, E. E.; Brewer, S. H. Modulating Accidental Fermi Resonance: What a Difference a Neutron Makes. *J. Phys. Chem. Lett.* **2011**, *2*, 1672−1676.
(51) Leitner, D. M. Energy Flow in Proteins. *Annu. Rev. Phys. Chem.* **2008**, *59*, 233−259.
(52) Chin, J. W.; Santoro, S. W.; Martin, A. B.; King, D. S.; Wang, L.; Schultz, P. G. Addition of P-Azido-L-Phenylalanine to the Genetic Code of Escherichia Coli. *J. Am. Chem. Soc.* **2002**, *124*, 9026−9027.
(53) Ye, S.; Zaitseva, E.; Caltabiano, G.; Schertler, G. F. X.; Sakmar, T. P.; Deupi, X.; Vogel, R. Tracking G-Protein-Coupled Receptor Activation Using Genetically Encoded Infrared Probes. *Nature* **2010**, *464*, 1386−1390.
(54) Kim, Y.; Ho, S. O.; Gassman, N. R.; Korlann, Y.; Landorf, E. V.; Collart, F. R.; Weiss, S. Efficient Site-Specific Labeling of Proteins Via Cysteines. *Bioconjugate Chem.* **2008**, *19*, 786−791.
(55) Perera, S. M.; Aikawa, T.; Shaner, S. E.; Moran, S. D.; Wang, L. Effects of Intramolecular Group and Solvent on Vibrational Coupling Modes and Strengths of Fermi Resonances in Aryl Azides: A Dft Study of 4-Azidotolune and 4-Azido-N-Phenylmaleimide. *ChemRxiv* **2022**, DOI: 10.26434/chemrxiv-2022-gd3mk. (accessed 2023−08−08).
(56) Park, J. Y.; Mondal, S.; Kwon, H.-J.; Sahu, P. K.; Han, H.; Kwak, K.; Cho, M. Effect of Isotope Substitution on the Fermi Resonance and Vibrational Lifetime of Unnatural Amino Acids

Modified with Ir Probe: A 2d-Ir and Pump-Probe Study of 4-Azido-L-Phenyl Alanine. *J. Chem. Phys.* **2020**, *153*, 164309.
(57) Shao, N.; Singh, N. S.; Slade, S. E.; Jones, A. M. E.; Balasubramanian, M. K. Site Specific Genetic Incorporation of Azidophenylalanine in Schizosaccharomyces Pombe. *Sci. Rep.* **2015**, *5*, 17196.
(58) Lukasak, B.; Morihiro, K.; Deiters, A. Aryl Azides as Phosphine-Activated Switches for Small Molecule Function. *Sci. Rep.* **2019**, *9*, 1470.
(59) Hajipour, A. R.; Mohammadsaleh, F. Synthesis of Aryl Azides from Aryl Halides Promoted by Cu2O/Tetraethylammonium Prolinate. *Tetrahedron Lett.* **2014**, *55*, 6799−6802.
(60) Spivey, K.; Williams, J. I.; Wang, L. Structures of Undercagold Clusters: Ligand Effect. *Chem. Phys. Lett.* **2006**, *432*, 163−166.
(61) Mitra, S.; Khuu, T.; Choi, T. H.; Huchmala, R. M.; Jordan, K. D.; McCoy, A. B.; Johnson, M. A. Vibrational Signatures of HNO_3 Acidity When Complexed with Microhydrated Alkali Metal Ions, $M^+ \cdot (HNO_3)(H2O)_{n=5}$ (M = Li, K, Na, Rb, Cs), at 20 K. *J. Phys. Chem. A* **2022**, *126*, 1640−1647.
(62) Steinkellner, G.; Gruber, C. C.; Pavkov-Keller, T.; Binter, A.; Steiner, K.; Winkler, C.; Lyskowski, A.; Schwamberger, O.; Oberer, M.; Schwab, H.; et al. Identification of Promiscuous Ene-Reductase Activity by Mining Structural Databases Using Active Site Constellations. *Nat. Commun.* **2014**, *5*, 4150.
(63) Baiz, C. R.; Blasiak, B.; Bredenbeck, J.; Cho, M.; Choi, J.-H.; Corcelli, S. A.; Dijkstra, A. G.; Feng, C.-J.; Garrett-Roe, S.; Ge, N.-H.; et al. Vibrational Spectroscopic Map, Vibrational Spectroscopy, and Intermolecular Interaction. *Chem. Rev.* **2020**, *120*, 7152−7218.
(64) Barone, V. Anharmonic Vibrational Properties by a Fully Automated Second-Order Perturbative Approach. *J. Chem. Phys.* **2005**, *122*, No. 014108.
(65) Piccardo, M.; Bloino, J.; Barone, V. Generalized Vibrational Perturbation Theory for Rotovibrational Energies of Linear, Symmetric and Asymmetric Tops: Theory, Approximations, and Automated Approaches to Deal with Medium-to-Large Molecular Systems. *Int. Quant. Chem.* **2015**, *115*, 948−982.
(66) Pandey, H. D.; Leitner, D. M. Vibrational States and Nitrile Lifetimes of Cyanophenylalanine Isotopomers in Solution. *J. Phys. Chem. A* **2018**, *122*, 6856−6863.
(67) Fujisaki, H.; Yagi, K.; Hirao, K.; Straub, J. E. Quantum Dynamics of N-Methylacetamide Studied by the Vibrational Configuration Interaction Method. *Chem. Phys. Lett.* **2007**, *443*, 6−11.
(68) Frisch, M. J.; Trucks, G. W.; Schlegel, H. B.; Scuseria, G. E.; Robb, M. A.; Cheeseman, J. R.; Scalmani, G.; Barone, V.; Peterson, G. A.; Nakatsuji, H. *Gaussian 16 Rev. C.01*: Wallingford, CT, 2016.
(69) Perera, S. M.; Wang, L. DFT Studies of Rotational Conformers of 4-Azido-N-Phenylmalemide. *ChemRxiv* **2023**, DOI: 10.26434/chemrxiv-2023-bw143. (accessed 2023−08−08).
(70) Gong, K.; Xu, F.; Zhao, Z.; Li, W.; Liu, D.; Zhou, X.; Wang, L. Theoretical Investigation on Functional Group Modulation of Uv-Vis Absorption Profiles of Triphenylamine Derivatives. *Phys. Chem. Chem. Phys.* **2023**, *25*, 22002−22010.
(71) Walkup, L. L.; Weerasinghe, K. C.; Tao, M.; Zhou, X.; Zhang, M.; Liu, D.; Wang, L. Importance of Dynamics in Electron Excitation and Transfer of Organic Dyes. *J. Phys. Chem. C* **2010**, *114*, 19521−19528.
(72) Janjua, M. R. S. A.; Mahmood, A.; Ahmad, F. Solvent Effects on Nonlinear Optical Response of Certain Tetramminеruthenium(Ii) Complexes of Modified 1,10-Phenanthrolines. *Can. J. Chem.* **2013**, *91*, 1303−1309.
(73) Xu, F.; Testoff, T. T.; Wang, L.; Zhou, X. Cause, Regulation and Utilization of Dye Aggregation in Dye-Sensitized Solar Cells. *Molecules* **2020**, *25*, 4478.
(74) Sun, H.; Liu, D.; Wang, T.; Lu, T.; Li, W.; Ren, S.; Hu, W.; Wang, L.; Zhou, X. Enhanced Internal Quantum Efficiency in Dye-Sensitized Solar Cells: Effect of Long-Lived Charge-Separated State of Sensitizers. *ACS Appl. Mater. Interfaces* **2017**, *9*, 9880−9891.
(75) Xu, F.; Gong, K.; Liu, D.; Wang, L.; Li, W.; Zhou, X. Enhancing Photocurrent of Dye-Sensitized Solar Cells through Solvent Modulating Aggregation of Dyes. *Sol. Energy* **2022**, *240*, 157−167.
(76) Xu, F.; Gong, K.; Fan, W.; Liu, D.; Li, W.; Wang, L.; Zhou, X. J-Aggregated Dyes for Dye-Sensitized Solar Cells: Suppressing Aggregation-Induced Excited-State Quenching by Intramolecular Charge Separation. *ACS Appl. Energy Mater.* **2022**, *5*, 13780−13790.
(77) Lin, T.; Zhang, W.; Wang, L. Theoretical Calculation of Separation Factors for Boron Isotopic Exchange between Bf_3 and $Bf_3 \cdot C_6h_5och_3$. *J. Phys. Chem. A* **2009**, *113*, 7267−7274.
(78) Lin, T.; Zhang, W.; Wang, L. Complex Formation between Anisole and Boron Trifluoride: Structural and Binding Properties. *J. Phys. Chem. A* **2008**, *112*, 13600−13608.
(79) Wang, T.; Zhao, C.; Zhang, L.; Lu, T.; Sun, H.; Bridgmohan, C. N.; Weerasinghe, K. C.; Liu, D.; Hu, W.; Li, W.; et al. Enhancing Photoinduced Charge Separation through Donor Moiety in Donor-Accepter Organic Semiconductors. *J. Phys. Chem. C* **2016**, *120*, 25263−25275.
(80) Wang, T.; Weerasinghe, K. C.; Ubaldo, P. C.; Liu, D.; Li, W.; Zhou, X.; Wang, L. Tuning Electron−Hole Distance of the Excitons in Organic Moleculesusing Functional Groups. *Chem. Phys. Lett.* **2015**, *618*, 142.
(81) Arulaabaranam, K.; Muthu, S.; Mani, G.; Irfan, A. Conformational Study, Ft-Ir, Ft-Raman, Solvent Effect on Uv−Vis, Charge Transfer and Protein−Ligand Interactions of Methyl-2-Pyrazinecarboxylate. *J. Mol. Liq.* **2021**, *341*, No. 116934.
(82) Latosińska, J. N.; Latosińska, M.; Tomczak, M. A.; Medycki, W. Conformational Stability and Thermal Pathways of Relaxation in Triclosan (Antibacterial/Excipient/Contaminant) in Solid-State: Combined Spectroscopic (^{1}H NMR) and Computational (Periodic DFT) Study. *J. Phys. Chem. A* **2015**, *119*, 4864−4874.
(83) Dorotíková, S.; Plevova, K.; Bucinsky, L.; Malcek, M.; Herich, P.; Kuckova, L.; Bobenicova, S.; Soralova, S.; Kozisek, J.; Fronc, M.; et al. Conformational, Spectroscopic, and Molecular Dynamics DFT Study of Precursors for New Potential Antibacterial Fluoroquinolone Drugs. *J. Phys. Chem. A* **2014**, *118*, 9540−9551.
(84) Zaier, R.; Ayachi, S. DFT Molecular Modeling Studies of D-Π-A-Π-D Type Cyclopentadithiophene-Diketopyrrolopyrrole Based Small Molecules Donor Materials for Organic Photovoltaic Cells. *Optik* **2021**, *239*, No. 166787.
(85) Irfan, A.; Chaudhry, A. R.; Al-Sehemi, A. G. Electron Donating Effect of Amine Groups on Charge Transfer and Photophysical Properties of 1,3-Diphenyl-1h-Pyrazolo[3,4-B]Quinolone at Molecular and Solid State Bulk Levels. *Optik* **2020**, *208*, No. 164009.
(86) Irfan, A.; Al-Sehemi, A. G.; Assiri, M. A.; Ullah, S. Exploration the Effect of Metal and Electron Withdrawing Groups on Charge Transport and Optoelectronic Nature of Schiff Base Ni(II), Cu(II) and Zn(II) Complexes at Molecular and Solid-State Bulk Scales. *Mater. Sci. Semicond. Process.* **2020**, *107*, No. 104855.
(87) Sandeli, A. E.-K.; Khiri-Meribout, N.; Benzerka, S.; Boulebd, H.; Gurbuz, N.; Ozdemire, N.; Ozdemir, I. Synthesis, Structures, Dft Calculations, and Catalytic Application in the Direct Arylation of Five-Membered Heteroarenes with Aryl Bromides of Novel Palladium-N-Heterocyclic Carbene Peppsi-Type Complexes. *New J. Chem.* **2021**, *45*, 17878.
(88) Irfana, A.; Chaudhry, A. R.; Al-Sehemi, A. G.; Assiri, M. A.; Hussain, A. Charge Carrier and Optoelectronic Properties of Phenylimidazo[1,5-a] Pyridine-Containing Small Molecules at Molecular and Solid-State Bulk Scales. *Comput. Mater. Sci.* **2019**, *170*, No. 109179.
(89) Divya, V. V.; Suresh, C. H. Design and Dft Study of Nitrogen-Rich Donor Systems for Improved Photovoltaic Performance in Dye-Sensitized Solar Cells. *New J. Chem.* **2021**, *45*, 11585.
(90) Wang, T.; Weerasinghe, K. C.; Sun, H.; Hu, X.; Lu, T.; Liu, D.; Hu, W.; Li, W.; Zhou, X.; Wang, L. Effect of Triplet State on the Lifetime of Charge Separation in Ambipolar D-A_1-A_2 Organic Semiconductors. *J. Phys. Chem. C* **2016**, *120*, 11338−11349.
(91) Yang, J.; Liu, D.; Lu, T.; Sun, H.; Li, W.; Testoff, T. T.; Zhou, X.; Wang, L. Effects of Heterocyclic Ring and Amino-Ethyl-Amino

Group on the Electronic and Photophysical Properties of a Triphenylamine-Pyrimidine Dye. *Int. J. Quantum Chem.* **2020**, *120*, No. e26355.
(92) Miao, B.; Wu, Z.-P.; Xu, H.; Zhang, M.; Chen, Y.; Wang, L. DFT Studies on the Key Competing Reaction Steps Towards Complete Ethanol Oxidation on Transition Metal Catalysts. *Comput. Mater. Sci.* **2019**, *156*, 175−186.
(93) Miao, B.; Wu, Z.; Xu, H.; Zhang, M.; Chen, Y.; Wang, L. Ir Catalysts: Preventing CH_3COOH Formation in Ethanol Oxidation. *Chem. Phys. Lett.* **2017**, *688*, 92−97.
(94) Xu, H.; Miao, B.; Zhang, M.; Chen, Y.; Wang, L. Mechanism of C−C and C−H Bond Cleavage in Ethanol Oxidation Reaction on $Cu_2O(111)$: A DFT-D and DFT+U Study. *Phys. Chem. Chem. Phys.* **2017**, *19*, 26210−26220.
(95) Wu, R.; Wang, L. A Density Functional Theory Study on the Mechanism of Complete Ethanol Oxidation on Ir(100): Surface Diffusion-Controlled C-C Bond Cleavage. *J. Phys. Chem. C* **2020**, *124*, 26953−26964.
(96) Wu, C.; Wang, L.; Xiao, Z.; Li, G.; Wang, L. Understanding Deep Dehydrogenation and Cracking of N-Butane on Ni(111) by a DFT Study. *Phys. Chem. Chem. Phys.* **2020**, *22*, 724−733.
(97) Gong, K.; Yang, J.; Testoff, T. T.; Li, W.; Wang, T.; Liu, D.; Zhou, X.; Wang, L. Electronically Excited State Structures and Stabilities of Organic Small Molecules: A DFT Study of Triphenylamine Derivatives. *Chem. Phys.* **2021**, *549*, No. 111256.
(98) Mahmood, A.; Wang, J.-L. A Time and Resource Efficient Machine Learning Assisted Design of Non-Fullerene Small Molecule Acceptors for P3ht-Based Organic Solar Cells and Green Solvent Selection. *J. Mater. Chem. A* **2021**, *9*, 15684.
(99) Mahmood, A.; Irfan, A.; Wang, J.-L. Developing Efficient Small Molecule Acceptors with Sp2-Hybridized Nitrogen at Different Positions by Density Functional Theory Calculations Molecular Dynamics Simulations and Machine Learning. *Chem. − Eur. J.* **2022**, *28*, No. e202103712.
(100) Mahmood, A.; Irfan, A.; Wang, J.-L. Machine Learning and Molecular Dynamics Simulation-Assisted Evolutionary Design and Discovery Pipeline to Screen Efficient Small Molecule Acceptors for Ptb7-Th-Based Organic Solar Cells with over 15% Efficiency. *J. Mater. Chem. A* **2022**, *10*, 4170.
(101) Mahmood, A.; Khan, S. U.-D.; Rehman, F. U. Assessing the Quantum Mechanical Level of Theory for Prediction of Uv/Visible Absorption Spectra of Some Aminoazobenzene Dyes. *J. Saudi Chem. Soc.* **2015**, *19*, 436−441.
(102) Walkup, L. L.; Weerasinghe, K. C.; Tao, M.; Zhou, X.; Zhang, M.; Liu, D.; Wang, L. Importance of Dynamics in Electron Excitation and Transfer of Organic Dyes. *J. Phys. Chem. C* **2010**, *114*, 19521−19528.
(103) Hudson, G. A.; Cheng, L.; Yu, J.; Yan, Y.; Dyer, D. J.; McCarroll, M. E.; Wang, L. Computational Studies on Response and Binding Selectivity of Fluorescence Sensors. *J. Phys. Chem. B* **2010**, *114*, 870−876.
(104) Wang, T.; Weerasinghe, K. C.; Liu, D.; Li, W.; Yan, X.; Zhou, X.; Wang, L. Ambipolar Organic Semiconductors with Cascades of Energy Levels for Generating Long-Lived Charge Separated States: A Donor−Acceptor1−Acceptor2 Architectural Triarylamine Dye. *J. Mater. Chem. C* **2014**, *2*, 5466−5470.
(105) Yang, Q.; Mendolicchio, M.; Barone, V.; Bloino, J. Accuracy and Reliability in the Simulation of Vibrational Spectra: A Comprehensive Benchmark of Energies and Intensities Issuing from Generalized Vibrational Perturbation Theory to Second Order (GVPT2). *Front. Astronomy Space Sci.* **2021**, *8*, No. 665232.
(106) Nielsen, H. H. The Vibration-Rotation Energies of Molecules. *Rev. Mod. Phys.* **1951**, *23*, 90−136.
(107) Schmitz, A. J.; Pandey, H. D.; Chalyavi, F.; Shi, T.; Fenlon, E. E.; Brewer, S. H.; Leitner, D. M.; Tucker, M. J. Tuning Molecular Vibrational Energy Flow within an Aromatic Scaffold Via Anharmonic Coupling. *J. Phys. Chem. A* **2019**, *123*, 10571−10581.

https://doi.org/10.1021/acs.jpca.3c06312
J. Phys. Chem. A 2023, 127, 8911−8921